Research paper

Numerical and theoretical research on spatial shear lag effect of self-anchored suspension bridge steel box girder

Yanfeng Li[1], Ying He[2], Longsheng Bao[3], Baoyun Sun[4], Qinghe Wang[5]

Abstract: The shear lag effect of the steel box girder section in a self-anchored suspension bridge was investigated in this study. Finite element analysis software Midas Civil was used to discretize the girder under analysis into space plate elements and establish a plate element model. The law of shear lag in the longitudinal direction of the girder in the construction and completion stages was determined accordingly. The shear lag coefficient appears to change suddenly near the side support, middle support, side cable anchorage area, and near the bridge tower support of the steel box girder under the imposed load. The most severe shear lag effect is located near the side support and near the side cable anchorage area. Steel box girder sections are simulated before and after system conversion to analyze the shear lag coefficient in the bridge construction stage. The results show that the shear lag coefficient markedly differs before versus after system conversion due to the different stress mechanisms. The finite element analysis results were validated by comparison with the results of an analysis via analogous rod method.

Keywords: self-anchored suspension bridge, steel box girder, shear lag effect, finite element analysis

---

[1] Prof., PhD., School of Transportation Engineering, Shenyang Jianzhu University, Shenyang 110168, China, e-mail: lyfneu@126.com, ORCID: https://orcid.org/0000-0003-2153-7934
[2] DSc., School of Transportation Engineering, Shenyang Jianzhu University, Shenyang 110168, China, e-mail: hying9999@126.com, ORCID: https://orcid.org/0000-0003-0489-9044
[3] Prof., PhD., School of Transportation Engineering, Shenyang Jianzhu University, Shenyang 110168, China, e-mail: 13516094255@163.com, ORCID: https://orcid.org/0000-0001-5582-1103
[4] Prof., PhD., School of Transportation Engineering, Shenyang Jianzhu University, Shenyang 110168, China, e-mail: Sby6@sina.com, ORCID: https://orcid.org/0000-0003-3260-3386
[5] Prof., PhD., School of Transportation Engineering, Shenyang Jianzhu University, Shenyang 110168, China, e-mail: wangqinghe@sjzu.edu.cn, ORCID: https://orcid.org/0000-0002-1530-4555

1. Introduction

Steel box girders are widely used in the bridge engineering field due to their light weight, high strength, convenient splicing, simple construction, good overall force conditions, and smooth appearance. When the steel box girder of a self-anchored suspension bridge is placed under compressive and bending loads, the shear lag effect of its flange grows severe and the normal stress acting upon the structure is very complicated [1] [2] [3]. Shear lag is one of the main causes of cracks [4] [5] [6]. The effective width is used instead of the actual flange width when considering the effects of shear lag on the box girder. The bridge codes of various countries stipulate effective width calculations for specific structures such as simply supported beams, continuous beams, and cantilever beams, but there is no clear provision for the steel box girders of self-anchored suspension bridges. Especially for bridges with relatively large spans, the shear lag effect of the steel box girder at each fulcrum is increasingly prominent when the moment of inertia of the slab is relatively large [7] [8] [9]. There has been a great deal of research on the shear lag effect in steel box girders to date. Guo et al. used the finite element method to calculate the shear lag coefficient of a steel box girder with different stiffeners [10]. Zhao et al. used an indoor model test method to study the shear lag effect of a continuous steel box girder bridge with large curvature under load [11]. Zhu et al. studied the influence of width-span ratio, supporting length, roof thickness, suspension wing ratio, and number of diaphragms on the shear lag of a corrugated steel web box girder [12] [13]. Zhou and Ma et al. used multiple parabolas as the longitudinal warping displacement difference function to obtain an analytical solution for the shear lag effect of composite beams with corrugated steel webs [14] [15]. Chen et al. studied the influence of various factors on the shear lag effect of composite box girder bridges with corrugated steel webs [16]. Zou et al. analyzed the shear lag effect of a prestressed concrete curved box girder with corrugated steel webs under different bearing arrangements [17]. Ni et al. used the spatial grid analysis method to analyze the horizontal and vertical distribution of the shear lag coefficient of the key sections of the side and mid span [18].

The above studies all center on the steel box girder under bending, there have been relatively few studies on the spatial stress of the steel box girder of self-anchored suspension bridges under compressive and bending loads. In fact, the key factors directly affecting the force and deformation of the structure generally show non-uniform distribution and random changes with the spatial position and action. Therefore, such engineered structures are actually non-uniform and non-linear complex systems [19] [20].

The shear lag effect of a self-anchored suspension bridge steel box girder section was examined in this study. The finite element analysis software Midas Civil was used to discretize the girder into space plate elements, then a plate element model was established to systematically analyze the spatial shear lag effect law of the girder in the bridge construction stage and bridge completion stage. The results of this work have certain reference significance for similar projects.

2. Research background

The main span of the self-anchored suspension bridge analyzed in this study is 40+90+220+90+40=480 m. The main girder is a whole steel box girder. The top of the girder is an orthotropic plate structure. The elevation layout of the bridge is shown in Figure 1. The steel box girder has an integral flat box section with cantilevers arms. The section width of the girder across the cable area of the main bridge is 43.3 m. The bridge tower position is locally widened to 48 m, the beam height is 3 m, and the anchorage beam height is locally thickened to 4.8 m. The cross-section width of the girder in the cable-free zone of the counterweight span is 40 m and the beam height is 2.3 m. A cross-sectional schematic diagram of the structure is shown in Figure 2.
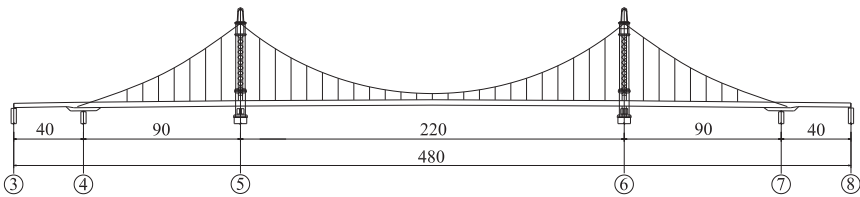
Figure 1: Elevation of main bridge (unit: m)
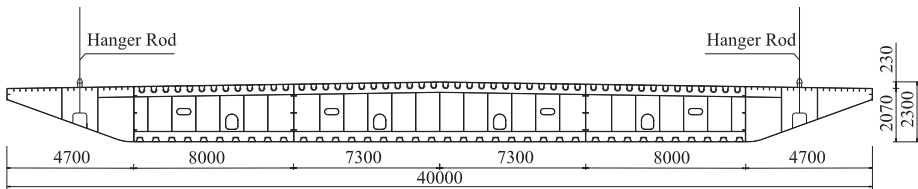
(a) Transverse partition
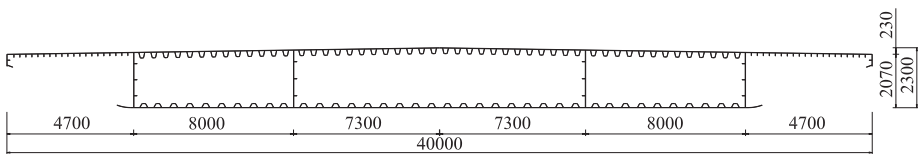
(b) Non-transverse partition

Figure 2: Schematic diagram of beam cross-section

3. Spatial finite element model establishment of self-anchored suspension bridge

The finite element software Midas Civil was used to establish the space plate shell model of the self-anchored suspension bridge. The plate element was used to establish the main bridge steel box girder part, the tension element is used to establish the hanging cable part, and the rest were all established as beam elements. The model was divided into 65,412 nodes and 74,699 elements including 154 tension-only elements, 1,408 beam elements, and 73,137 plate elements. The space plate and shell element model are shown in Figures 3 and 4.

Figure 3: Space plate and shell element model
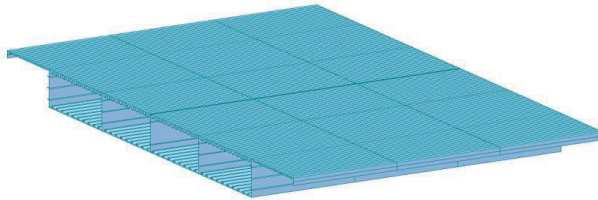
Figure 4: Schematic diagram of portion of shell element model

4. Lag effect on girder during bridge construction process

The forces acting on the main girder section of cable-stayed bridge are highly complex, and the bridge construction process is highly dynamic. The stress in the main girder section of different working conditions and different beam sections is different [21-23]. The key nodes on the edge of the main girder cross-section were isolated to analyze the shear lag coefficient distribution law along the longitudinal direction of the upper edge of the main girder section during the construction stage. For convenience, the key points were marked with capital English letters: point A, point C, and point E are points at the junction of the web and the roof, and points B and D are located in the middle of each cell of the box girder. The horizontal position of each point is shown in Figure 5. The analysis

was focused on the longitudinal shear lag effect of girder section before and after the system conversion.
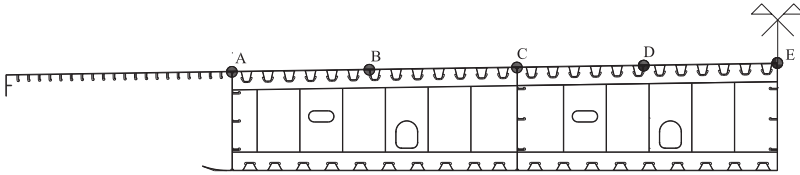
Figure 5: Schematic diagram of cross-section key points

4.1 Division of girder construction conditions

The main girder of the bridge was constructed via the single-side incremental launching method with the push-in platform placed on the shore. The single girder production is divided into three stages: unit production, in-situ steel girder assembly pre-assembly, and steel girder site installation. The steel beams are pre-assembled by continuous matching under the installation sequence requirements. The full bridge is divided into five rounds for manufacturing, the continuous matching pre-assembly is completed and then decomposed into components. During the pushing process, three temporary piers are set up in the mid-span. The longitudinal position of the temporary piers is shown in Figure 6. The main cable catwalk has a separated structure: one end is anchored on the beam surface and the other is anchored on the top of the tower. Devices are installed on both sides of the tower top to adjust the construction sag as necessary.

Prefabricated parallel steel wire strands are erected one-by-one to complete the main cable. The hanging cable near the tower is first installed with a tower crane and a steel beam-topped vehicle is used for the mid-span area. The tower crane and the vehicle cannot be listed by the electric hoist hanging on the traction load-bearing cable for installation. The installation sequence of the hanging cable is the same as the tension sequence of the boom. After the hanging cable is installed, the lower anchor head is inserted into the corresponding steel anchor box of the main beam.

The main construction steps can be summarized as follows.

1) Complete the substructure, arrange temporary piers, and build a jacking platform on one side.

2) Push up the steel beam and close the main beam after the installation of the guide beam and auxiliary truss is complete.

3) Erect the main cable, install the hanging cable, and initially tension the hanging cable to form a self-anchored suspension bridge system.

4) Install the bridge deck components in order and pour the wet joints.

5) Remove the temporary pier, install the auxiliary structure, and adjust the cable force value to reach the design value.
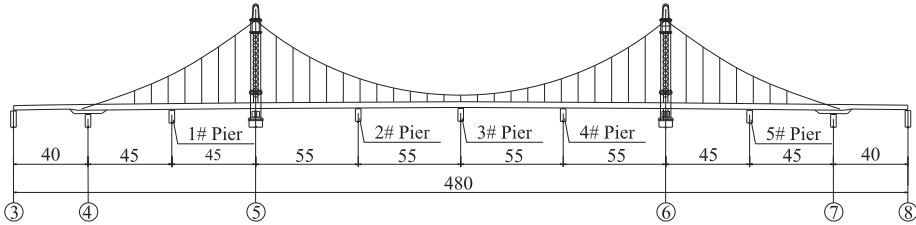
Figure 6: Longitudinal position of temporary piers (unit: m)

In the self-anchored suspension bridge construction process, the system conversion step is the most important. The closed multi-span continuous stiffening beam was considered in this study to characterize the initial state, the system conversion is completed by stretching the hanging cable. The self-weight of the stiffening beam is borne by the temporary support and transferred to the main cable through the hanging cable during system conversion. The main cable changes from the empty cable shape to the bridge shape. The internal force of the bridge structure itself changes accordingly, as does the shear lag coefficient of the main girder.

We analyzed the longitudinal shear lag effect of different bridge systems before and after system conversion to clearly illustrate this change trend. The specific working conditions were as follows.

Condition 1: The change law of the shear lag effect of the main girder along the longitudinal bridge direction during the main girder closing stage.

Condition 2: The change law of the shear lag effect of the main girder along the longitudinal bridge direction at the initial hanging cable tension stage.

4.2 Spatial shear lag effect of main girder (Condition 1)

A section was selected every 3 m in the longitudinal bridge direction and the key nodes of the box girder cross section were analyzed along the longitudinal bridge direction. In the longitudinal position, point 1 corresponds to pier 3#, point 7 corresponds to the temporary support, point 15 corresponds to pier 4#, point 16 falls near the side cable anchorage area, and point 40 corresponds to bridge tower 5#. Numeric point 53 corresponds to the mid-span. The structure is symmetrical, so only half of it was selected for shear lag analysis here.

The shear lag effect of each point was obtained after the finite element calculation and expanded along the longitudinal bridge direction to obtain the distribution law of the longitudinal shear lag coefficient at each point of the steel box girder during the main girder closing stage. (That is, the main beam was in a multi-span continuous stage in this case.)
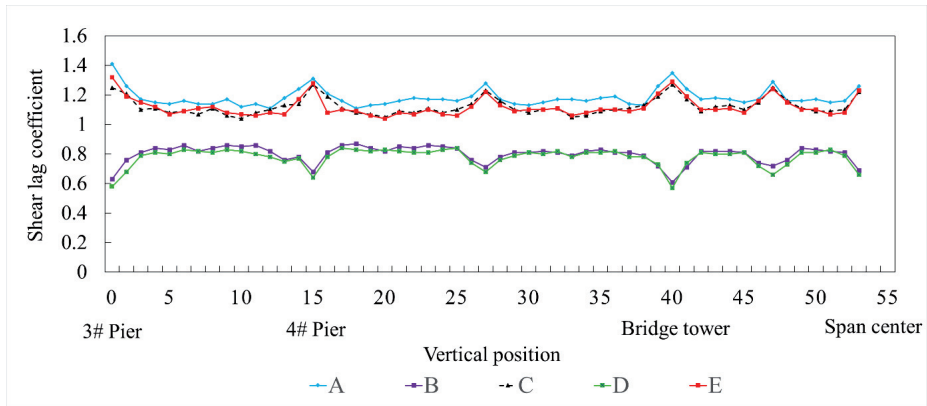
Figure 7: Longitudinal distribution of shear lag coefficient of steel box girder during main girder closure

The shear lag coefficient in the longitudinal direction of the steel box girder varies from 1.11 to 1.41 at point A, 0.61 to 0.87 at point B, 1.04 to 1.27 at point C, 0.57 to 0.84 at point D, and 1.04-1.32 at point E. The stress value at the junction of the web and the roof (points A, C, and E) during the main girder closing stage is greater than the elementary theoretical value of the beam, showing a positive shear lag effect. In the middle of the box room of the steel box girder (points B and D), the stress value is smaller than the theoretical value, showing a negative shear lag effect. The most obvious position of the shear lag coefficient is near the end of the girder, where the shear lag coefficient at point A is the largest at 1.41. There is also obvious shear lag effect near the bridge support location and at the temporary pier location. This is because the weight of the main girder at this stage is shared by the bridge support and the temporary support.

4.3 Spatial shear lag effect of main girder (Condition 2)

After the steel girder pushing is completed, the main cables and hanging cables are installed. The hanging cables are stretched to form a self-anchored suspension bridge structure system with a certain level of rigidity, then the system conversion is complete. At this time, the role of temporary piers is largely replaced by the main cable. The vertical load is transmitted to the main cable by the hanging cable and the main cable bears the tension.

Again, the shear lag effect of each point was obtained by finite element calculation and expanded along the longitudinal bridge direction to obtain the distribution law of the longitudinal shear lag coefficient at each point of the girder during the initial tension of the hanging cable (that is, in the stage of forming a self-anchored suspension bridge structure system), as shown in Figure 8.
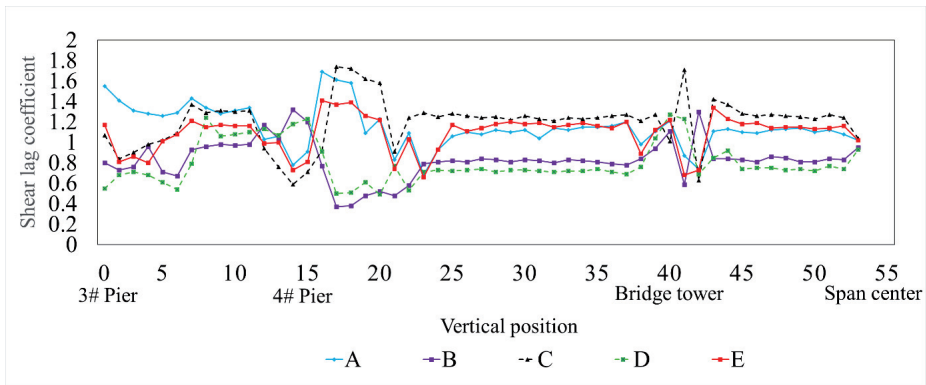
Figure 8: Longitudinal distribution of girder shear lag coefficient at initial hanging cable tension stage

The change area of the shear lag coefficient at each point in the longitudinal direction of the steel box girder is 0.68 to 1.69 at point A, 0.37 to 1.32 at point B, 0.59 to 1.74 at point C, 0.49 to 1.27 at point E, and 0.66 to 1.41 at point E. In the initial tensioning stage of the hanging cable, there are obvious positive shear lag effects at the three points A, C, and E near the end of the girder. The shear lag coefficient at point A is the largest, at 1.55. The shear lag coefficient changes significantly in the vicinity of the middle support and the side cable anchoring area, the positive shear lag effect response is strong at the three points A, C, and E. Among them, the positive shear lag effect at point C is the most severe at up to 1.74. At the bridge tower, the shear lag coefficient sharply changes again reaching its maximum value at point C, 1.71. At the mid-span position, the shear lag coefficient is relatively stable and its value does not significantly fluctuate.

Because different bridge systems have different force transmission mechanisms, there is a substantial difference in the shear lag coefficient of the main beam steel box girder before and after the system conversion. When the main girder is closed, the bridge system is a multi-span continuous system without cable force or other certain factors. When the main cable is erected and the hanging cables are stretched, the bridge system is transformed into a self-anchored suspension bridge system. The project has not been completed, but the entire system has taken shape. At this time, the force transmission method of the bridge aligns with that of the self-anchored suspension bridge, the vertical load is transmitted to the main cable by the hanging cable. The main cable bears the tensile force, which is then transmitted to the pylon and the main beam through the saddle and anchoring equipment on the top of the tower. The pulling force is mainly borne by the main cable and the horizontal force is mainly borne by the main beam.

5. Shear lag effect of girder in bridge completion stage

This section discusses the longitudinal shear lag effect of the steel box girder section under different loads at the bridge completion stage.

5.1 Longitudinal shear lag effect of steel box girder under uniform load

Figure 9 shows the distribution law of the longitudinal shear lag coefficient at each point of the steel box girder under a uniform load. As mentioned above, only half of the structure was subjected to shear lag analysis because it is symmetrical.
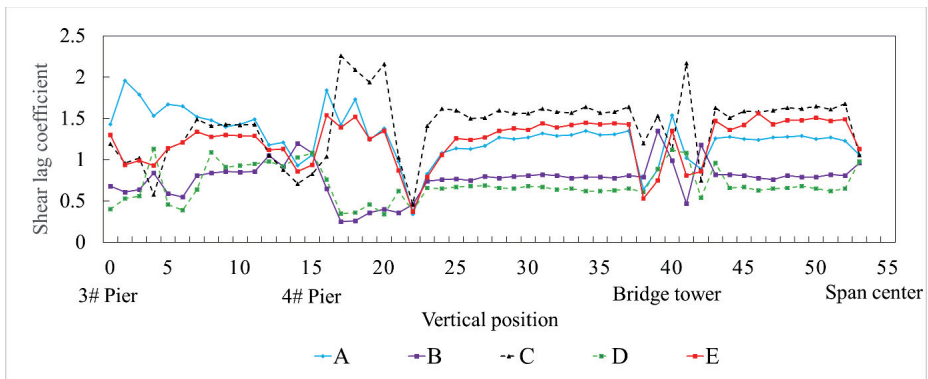
Figure 9: Longitudinal distribution of shear lag coefficient under uniform load

The shear lag coefficient in the longitudinal direction of the steel box girder varies from 0.34 to 1.96 at point A, 0.25 to 1.35 at point B, 0.46 to 2.26 at point C, 0.34 to 1.13 at point E, and at point E from 0.37 to 1.56. There are obvious positive shear lag effects at points A, C, and E near the end of the girder. The shear lag coefficient at point A is the largest at 1.43. As the shear lag coefficients of each point at the end of the beam began to change gradually, the shear lag coefficients of points A, C, and E decreased slightly at 1/4 of the side span of the main bridge while those at points B and D increased slightly. The shear lag coefficient of each point near the middle of the side span tends to be stable. The shear lag coefficient changes significantly in the vicinity of the middle support and side cable anchoring area, where serious positive shear lag effects emerge at points A, C, and E. Among them, the positive shear lag effect at point C is the most severe with a maximum value of 2.26. Between the anchorage area of the side cable of the main bridge and the support of the pylon, the shear lag coefficient tends to be stable and does not significantly fluctuate. There is a sudden change in the shear lag coefficient near the pylons, with a maximum value of 2.17 at point C. Near the mid-span, the shear lag coefficient tends to be stable and does not deviate from approximately 1.

5.2 Longitudinal shear lag effect of steel box girder under concentrated load

Figure 10 shows the distribution law of the longitudinal shear lag coefficient at each point of the steel box girder under a concentrated load.
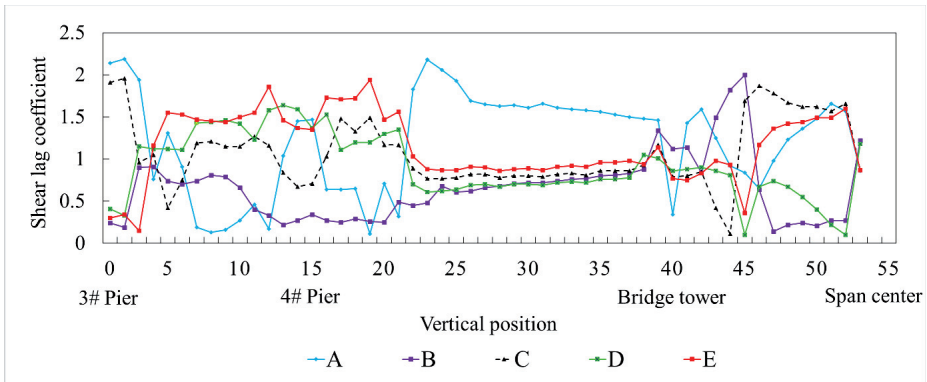
Figure 10: Longitudinal distribution of shear lag coefficient under concentrated load

The shear lag coefficient in the longitudinal direction of the steel box girder varies from 0.18 to 2.19 at point A, 0.21 to 2 at point B, 0.22 to 1.96 at point C, 0.2 to 1.64 at point D, and 0.17 to 1.94 at

point E. Under the action of concentrated load, there are obvious positive shear lag effects at the three points A, C, and E near the end of the steel box girder. The shear lag coefficient at point A is the largest at 2.14. The shear lag coefficient of each point at the end of the beam begins to to change as it gradually moves away from the end of the beam, the shear lag coefficient of each point stabilizes in the middle of the side span. There is a severe shear lag effect in the vicinity of the middle support, mainly at point E, with a maximum value of 1.94. This coefficient is stable between the anchorage area of the side cable of the main bridge and the support of the pylon, but the shear lag effect at point A is more severe. The shear lag coefficient at the position of the bridge tower also changes suddenly. Due to the influence of the concentrated load, the shear-shear lag effect of points A and E grows increasingly obvious in the direction of the mid-span.

5.3 Longitudinal shear lag effect of steel box girder under eccentric load

Figure 11 shows the distribution law of the longitudinal shear lag coefficient at each point of the steel box girder under an eccentric load.
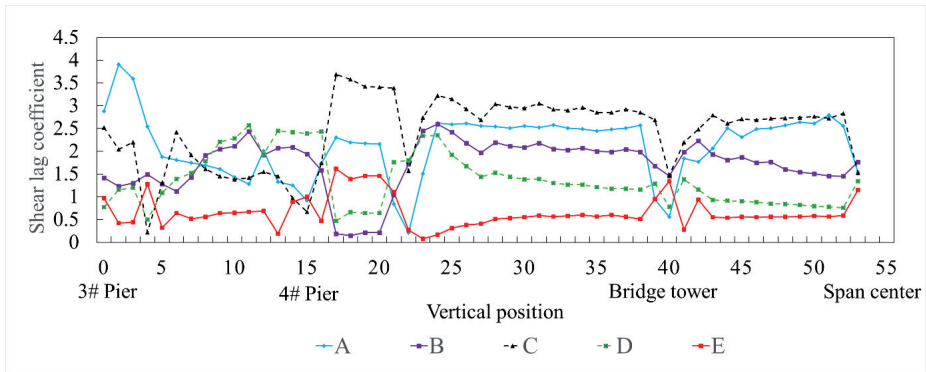
Figure 11: Longitudinal distribution of shear lag coefficient under eccentric load

The shear lag coefficient in the longitudinal direction of the steel box girder varies from 0.21 to 3.91 at point A, 0.24 to 2.6 at point B, 0.22 to 3.69 at point C, 0.47 to 2.57 at point D, and 0.18 to 1.62 at point E. Points A, C, and E near the end of the steel box girder show more obvious positive shear lag effects under the eccentric load, the shear lag coefficient at point A is the largest among them, at 2.88. At the middle position of each span, the shear lag coefficient of each point tends to be stable and does

not intensely fluctuate. In the vicinity of the middle support, the shear lag effect at point C is the most obvious with a maximum value of 2.26. There is a large fluctuation in the shear lag coefficient at the position where the pylon and the box girder of the main bridge are connected. The shear lag coefficient of each point at the mid-span position is around 1.5.

Based on the above analysis, we conclude that the bridge support is a position where the shear lag effect of the steel box girder is relatively intense. The side cable anchorage area shows a similarly intense shear lag effect as the bridge support. There is a certain degree of change in the shear lag coefficient near the 1/4 position of each span of the bridge, which approaches the junction of positive and negative stress values (that is, near the junction of positive and negative bending moments). The reaction force at the support abruptly induces the shear force, which peaks near the junction between the web and the top plate, so the normal bending stress excessive. In the side cable anchorage zone, the cable force causes local compression of the steel box girder section where the shear lag effect is particularly severe.

6. Analogous rod method for cross-section stress of single-box, four-chamber steel box girder under compressive and bending loads

Our finite element analysis indicates that in the side cable anchorage zone, cable force compresses the steel box girder section locally and the shear lag effect is serious. We considered the analogous rod method to have been used in the design of the thin-plate structures under analysis here. Each plate of the box girder is a combined system of the membrane and the main rod in this case, and a set of conditions is established according to the deformation coordination and balance conditions between the membrane and the rods. Differential equations are solved in combination with boundary conditions. Only one differential equation needs to be solved and the accuracy of the result satisfies practical engineering requirements. Similarly, we used the analogy bar method to analyze the shear lag effect acting on the cross-section of a single-box four-chamber steel box girder under compressive and bending loads.

6.1 Basic assumptions

We made four basic assumptions in conducting this analysis. 1) The thin-walled box girder is equivalent to a common force system composed of many idealized stiffeners and thin plates, as shown in Figure 12. 2) After equivalent treatment, the stiffeners in the compression range bear axial force

and the thin plate transmits shear force. 3) Based on the stress equivalence of the upper and lower flange plates of the box girder, the equivalent thickness of the thin plate and the sum of the equivalent area of the thin plate and equivalent front area of the stiffener is the equivalent area of the required stiffener. 4) The vertical shear force   acting on the section is borne by the web.
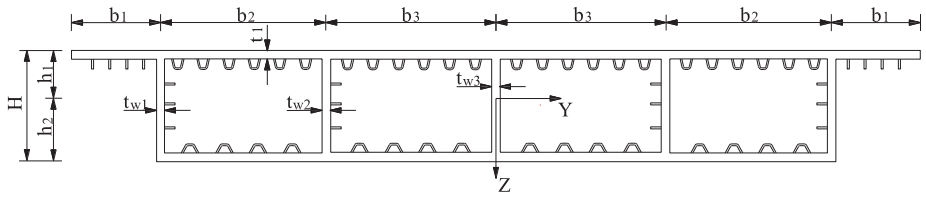
Figure 12: Single box four-chamber box girder section
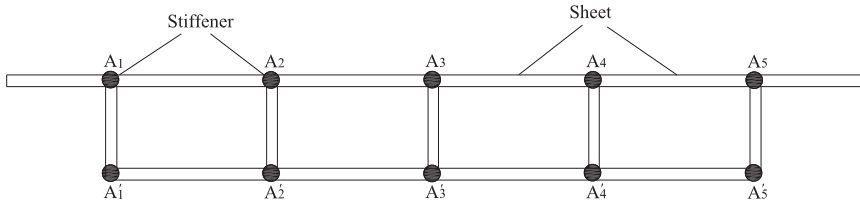
Figure 13: Thin plate and stiffener equivalent system

6.2 Equivalent calculation of thin plate and stiffener

When the bending moment M acts on a single-box, four-chamber box girder, the bending normal stress of the upper and lower wing plates can be determined according to the bending theory of elementary beams. The moment of inertia of the flange plate to itself is ignored and the following holds:

$$I = 2\left[\frac{(t_{w1}+t_{w2})H^3}{12}+(t_{w1}+t_{w2})H\left(\frac{H}{2}-h_1\right)^2\right]+\left[\frac{t_{w3}H^3}{12}+t_{w3}H\left(\frac{H}{2}-h_1\right)^2\right]+2\left[(b_1+b_2+b_3)t_1h_1^2\right]+2\left[(b_2+b_3)h_2^2\right] \quad (1)$$

The equivalent area of the upper and lower wings is:

$$\left.\begin{aligned}A_{ef(up)} &= 2\left[\alpha_1(t_{w1}+t_{w2})H+\beta_1 t_{w3}H+\eta_1(b_1+b_2+b_3)t_1\right]\\ A_{ef(down)} &= 2\left[\alpha_2(t_{w1}+t_{w2})H+\beta_2 t_{w3}H+\eta_2(b_2+b_3)t_2\right]\end{aligned}\right\} \quad (2)$$

The equivalent thickness of the upper and lower wings is:

$$\left.\begin{aligned} t_{ef(up)} &= \eta_1 t_1 \\ t_{ef(down)} &= \eta_2 t_2 \end{aligned}\right\} \tag{3}$$

The equivalent coefficient derived from Eqs. (1) and (2) is:

$$\left.\begin{aligned} \alpha_1 &= \frac{H}{12h_1} + \frac{1}{Hh_1}\left(\frac{H}{2} - h_1\right)^2, \quad \beta_1 = \frac{H}{12h_1} + \frac{1}{Hh_1}\left(\frac{H}{2} - h_1\right)^2, \quad \eta_1 = \frac{h_1}{H} + \frac{(b_2 + b_3)t_2 h_2^2}{(b_1 + b_2 + b_3)Ht_1 h_1} \\ \alpha_2 &= \frac{H}{12h_2} + \frac{1}{Hh_2}\left(\frac{H}{2} - h_1\right)^2, \, \beta_1 = \frac{H}{12h_2} + \frac{1}{Hh_2}\left(\frac{H}{2} - h_1\right)^2, \quad \eta_2 = \frac{(b_1 + b_2 + b_3)t_1 h_1^2}{(b_2 + b_3)Ht_2 h_2} + \frac{h_2}{H} \end{aligned}\right\} \tag{4}$$

According to the basic assumptions, the upper and lower wing plates are equivalent to a stiffening rod as shown in Figure 1. The area of each stiffening rod is shown in Table 1.

Table 1: Stiffener area formula table

Stiffener position	Stiffener number	Stiffener area formula
External rod of top plate	A_1、A_5	$\alpha_1 t_{w1} H + \eta_1\left(b_1 + \dfrac{b_2}{2}\right)t_1$
Top plate inner rod	A_2、A_4	$\alpha_1 t_{w2} H + \eta_1\left(\dfrac{b_2 + b_3}{2}\right)t_1$
Middle top pole	A_3	$\beta_1 t_{w3} H + \eta_1 b_3 t_1$
External rod of bottom plate	A_1'、A_5'	$\alpha_2 t_{w1} H + \eta_2\left(b_1 + \dfrac{b_2}{2}\right)t_2$
Internal rod of bottom plate	A_2'、A_4'	$\alpha_2 t_{w2} H + \eta_2\left(\dfrac{b_2 + b_3}{2}\right)t_2$
Middle rod of bottom plate	A_3'	$\beta_2 t_{w3} H + \eta_2 b_3 t_2$

6.3 Differential equations

Half of the width of the girder is taken as the research object here, as the structure is symmetrical. The stress state of the thin plate and stiffener is shown in Figure 14.
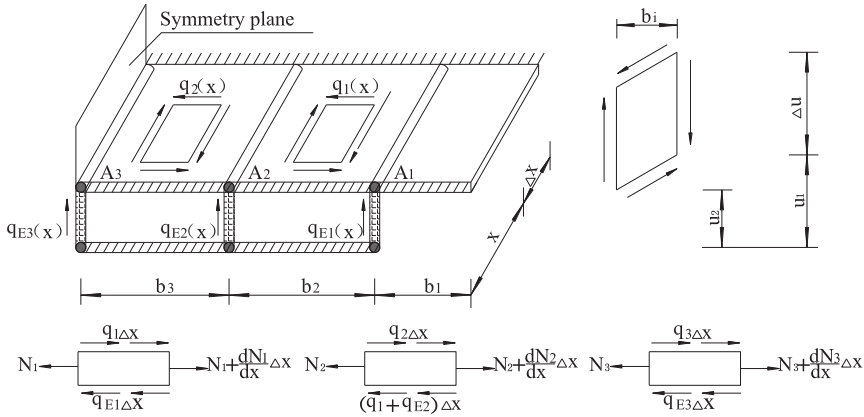
Figure 14: Single box four-chamber box girder top stiffener and force diagram

There are five stiffeners on the top and bottom plates. The balance equation of each stiffener can be established based on the force state of the micro-element body:

$$\frac{dN_1}{dx} = q_{E1}(x) - q_1(x); \frac{dN_2}{dx} = q_1(x) + q_{E2}(x) - q_2(x); \frac{dN_3}{dx} = q_{E3}(x) + 2q_2(x) \quad (5)$$

where $q_E(x)$ is the shear force of the web caused by the external load, $q_1(x)$ and $q_2(x)$ are the unknown shear flow of the equivalent thin plate between the No. 1 and No. 2 stiffeners and the No. 2 and No. 3 stiffeners, respectively.

Assuming that the vertical shear force at any section of the box girder is Q and the shear force flow is borne by the web, the shear force flow is distributed according to the principle of leverage:

$$q_{E1}(x) = \zeta_1 \frac{Q(x)H}{5H} = \frac{\zeta_1 Q(x)}{5}; \quad q_{E2}(x) = \zeta_2 \frac{Q(x)H}{5H} = \frac{\zeta_2 Q(x)}{5}; \quad q_{E3}(x) = \zeta_3 \frac{Q(x)H}{5H} = \frac{\zeta_3 Q(x)}{5} \quad (6)$$

where ζ_1, ζ_2, and ζ_3 are the shear coefficients of the outer, inner, and middle webs, respectively.

$$2(\zeta_1 + \zeta_2) + \zeta_3 = 1 \quad (7)$$

As shown in Figure 14, taking No. 1 and No. 2 stiffeners as examples, the shear angle change rate of the micro-block is:

$$\frac{d\gamma}{dx} = \frac{1}{b_2}\left(\frac{\partial u_1}{\partial x} - \frac{\partial u_2}{\partial x}\right) = \frac{1}{b_2}(\varepsilon_1 - \varepsilon_2) \text{ or } \frac{d\gamma}{dx} = \frac{1}{b_2 E}(\sigma_1 - \sigma_2) = \frac{1}{b_2 E}\left(\frac{N_1}{A_1} - \frac{N_2}{A_2}\right) \tag{8}$$

Formula $q = \gamma t_{ef(up)} G$ can be substituted into Formula (8) so that:

$$\frac{dq_1(x)}{dx} = \frac{Gt_{ef(up)}}{b_2 E}\left(\frac{N_1}{A_1} - \frac{N_2}{A_2}\right) \tag{9}$$

and thus:

$$\frac{dq_i(x)}{dx} = \frac{Gt_{ef(up)}}{b_{i+1}E}\left(\frac{N_i}{A_i} - \frac{N_{i+1}}{A_{i+1}}\right) \tag{10}$$

So for No. 2 and No. 3 stiffeners:

$$\frac{dq_2(x)}{dx} = \frac{Gt_{ef(up)}}{b_3 E}\left(\frac{N_2}{A_2} - \frac{N_3}{A_3}\right) \tag{11}$$

and the control differential equation can be obtained by combining Eqs. (9) and (11):

$$\left. \begin{array}{l} \dfrac{d^2q_1(x)}{d_2 x} - \dfrac{Gt_{ef(up)}}{b_2 E}\left(\dfrac{dN_1}{A_1 dx} - \dfrac{dN_2}{A_2 dx}\right) = 0 \\[3mm] \dfrac{d^2q_2(x)}{d_2 x} - \dfrac{Gt_{ef(up)}}{b_3 E}\left(\dfrac{dN_2}{A_2 dx} - \dfrac{dN_3}{A_3 dx}\right) = 0 \end{array}\right\} \tag{12}$$

Substituting Formula (5) into Formula (12) yields:

$$\left. \begin{array}{l} \dfrac{d^2q_1(x)}{d_2 x} - \dfrac{Gt_{ef(up)}}{b_2 E}\left[\left(-\dfrac{1}{A_1} - \dfrac{1}{A_2}\right)q_1(x) + \dfrac{1}{A_2}q_2(x)\right] = \dfrac{Gt_{ef(up)}}{b_2 E}\left[\dfrac{1}{A_1}q_{E1}(x) - \dfrac{1}{A_2}q_{E2}(x)\right] \\[3mm] \dfrac{d^2q_2(x)}{d_2 x} - \dfrac{Gt_{ef(up)}}{b_3 E}\left[\dfrac{1}{A_2}q_2(x) + \left(-\dfrac{1}{A_2} - \dfrac{2}{A_3}\right)q_2(x)\right] = \dfrac{Gt_{ef(up)}}{b_3 E}\left[\dfrac{1}{A_2}q_{E2}(x) - \dfrac{1}{A_3}q_{E3}(x)\right] \end{array}\right\} \tag{13}$$

and adding Eqs. (6) into (12) allows us to simplify it as:

$$\left. \begin{array}{l} \dfrac{d^2q_1(x)}{dx^2} + (c_{11} + c_{12})q_1(x) - c_{12}q_2(x) = (c_{11}\zeta_1 - c_{12}\zeta_2)\dfrac{Q(x)}{5} \\[3mm] \dfrac{d^2q_2(x)}{dx^2} + (c_{22} + c_{23})q_2(x) - c_{22}q_1(x) = \left(c_{22}\zeta_2 - \dfrac{c_{23}\zeta_3}{2}\right)\dfrac{Q(x)}{5} \end{array}\right\} \tag{14}$$

where $\varphi_i = \dfrac{Gt_{ef(up)}}{b_{i+1}E}$, $\phi_{ij} = \dfrac{\zeta_i}{A_j}(i,\ j=1,2)$, $c_{23} = \dfrac{2\varphi_2}{A_3}$.

6.4 Differential equation solving

We used the operator method to solve the differential equation. The matrix form of Eq. (14) is:

$$\begin{bmatrix} D^2 + c_{11} + c_{12} & -c_{12} \\ -c_{22} & D^2 + c_{22} + c_{23} \end{bmatrix} \begin{bmatrix} q_1(x) \\ q_2(x) \end{bmatrix} = \begin{bmatrix} c_{11}\zeta_1 - c_{12}\zeta_2 \\ c_{22}\zeta_2 - \dfrac{c_{23}\zeta_3}{2} \end{bmatrix} \frac{Q(x)}{5} \tag{15}$$

As per Cramer's Rule:

$$q_1(x) = \frac{\begin{vmatrix} c_{11}\zeta_1 - c_{12}\zeta_2 & -c_{12} & \dfrac{Q(x)}{5} \\ c_{22}\zeta_2 - \dfrac{c_{23}\zeta_3}{2} & D^2 + c_{22} + c_{23} \end{vmatrix}}{\begin{vmatrix} D^2 + c_{11} + c_{12} & -c_{12} \\ -c_{22} & D^2 + c_{22} + c_{23} \end{vmatrix}}$$

$$q_2(x) = \frac{\begin{vmatrix} D^2 + c_{11} + c_{12} & c_{11}\zeta_1 - c_{12}\zeta_2 & \dfrac{Q(x)}{5} \\ -c_{22} & c_{22}\zeta_2 - \dfrac{c_{23}\zeta_3}{2} \end{vmatrix}}{\begin{vmatrix} D^2 + c_{11} + c_{12} & -c_{12} \\ -c_{22} & D^2 + c_{22} + c_{23} \end{vmatrix}} \tag{16}$$

When a distributed and concentrated load is applied, the web bears all the corresponding shear flow, this shear flow at the web is evenly distributed along the vertical direction. $Q''(x) = 0$ and the shear function of the web is:

$$D^2 Q(x) = 0 \tag{17}$$

Substituting Eq. (17) into Eq. (16) reveals the unknown shear flow:

$$q_1(x) = \frac{\left[c_{11}(c_{22} + c_{23})\zeta_1 - c_{12}c_{23}\left(\zeta_2 + \dfrac{\zeta_3}{2} \right) \right] \dfrac{Q(x)}{5}}{(D^2 + c_{11} + c_{12})(D^2 + c_{22} + c_{23}) - c_{12}c_{22}}$$

$$q_2(x) = \frac{\left[c_{11}c_{22}(\zeta_1 + \zeta_2) - c_{23}(c_{11} + c_{12})\dfrac{\zeta_3}{2} \right] \dfrac{Q(x)}{5}}{(D^2 + c_{11} + c_{12})(D^2 + c_{22} + c_{23}) - c_{12}c_{22}} \tag{18}$$

Let $A = c_{11} + c_{12} + c_{23}$, $B = c_{11}c_{22} + c_{11}c_{23} + c_{12}c_{23}$, $C_1 = \dfrac{1}{5}\left[c_{11}(c_{22} + c_{23})\zeta_1 - c_{12}c_{23}\left(\zeta_2 + \dfrac{\zeta_3}{2} \right) \right]$ and

$C_2 = \dfrac{1}{5}\left[c_{11}c_{22}(\zeta_1 + \zeta_2) - c_{23}(c_{11} + c_{12})\dfrac{\zeta_3}{2} \right]$, then Eq. (18) can be simplified as:

$$D^4 q_1(x) + AD^2 q_1(x) + Bq_1(x) = C_1 Q(x) \atop D^4 q_2(x) + AD^2 q_2(x) + Bq_2(x) = C_2 Q(x) \Bigg\}$$ (19)

which is the fourth-order non-homogeneous equation with constant coefficients about "sum".

Let $\genfrac{}{}{0pt}{}{\alpha}{\beta} = \sqrt{\frac{1}{2}\left(-A \pm \sqrt{A_2 - 4B}\right)}$, then the general solution is:

$$q_1(x) = \chi_1 ch\alpha x + \chi_2 sh\alpha x + \chi_3 ch\beta x + \chi_4 sh\beta x + \frac{C_1}{B} Q(x) \atop q_2(x) = \varsigma_1 ch\alpha x + \varsigma_2 sh\alpha x + \varsigma_3 ch\beta x + \varsigma_4 sh\beta x + \frac{C_2}{B} Q(x) \Bigg\}$$ (20)

Constants χ_1, χ_2, χ_3, and χ_4 can be determined by the boundary condition. The constants ς_1, ς_2, ς_3, and ς_4 can be obtained by substituting "sum" into Eq. (14). The axial force of each stiffener can be obtained by substituting $q_1(x)$ and $q_2(x)$ into Eq. (5):

$$N_1 = -\frac{\chi_1}{\alpha} sh\alpha x - \frac{\chi_2}{\alpha} ch\alpha x - \frac{\chi_3}{\beta} sh\beta x - \frac{\chi_4}{\beta} ch\beta x + \left(\frac{\varsigma_1}{5} - \frac{C_1}{B}\right)\int Q(x)dx + \overline{C}_1$$

$$N_2 = \frac{\chi_1 - \varsigma_1}{\alpha} sh\alpha x + \frac{\chi_2 - \varsigma_2}{\alpha} ch\alpha x + \frac{\chi_3 - \varsigma_3}{\beta} sh\beta x + \frac{\chi_4 - \varsigma_4}{\beta} ch\beta x$$
$$\qquad + \left(\frac{\varsigma_2}{5} + \frac{C_1 - C_2}{B}\right)\int Q(x)dx + \overline{C}_2$$ (21)

$$N_3 = \frac{2\varsigma_1}{\alpha} sh\alpha x + \frac{2\varsigma_2}{\alpha} ch\alpha x + \frac{2\varsigma_3}{\beta} sh\beta x + \frac{2\varsigma_4}{\beta} ch\beta x + \left(\frac{\varsigma_3}{5} + \frac{2C_2}{B}\right)\int Q(x)dx + \overline{C}_3$$

where $\overline{C}_1$, $\overline{C}_2$, and $\overline{C}_3$ are constants and $\sigma_4 = \sigma_2$、$\sigma_5 = \sigma_1$. The stress of each stiffener is:

$$\sigma_i = \frac{N_i}{A_i} (i = 1,2,3)$$ (22)

6.5 Case analysis

The total section width of the single-box, four-chamber, simply supported steel box girder is B=43.3 m. The width of the cantilever plate is b_1=6.35 m, the width of the inner wing (outer bottom plate) is b_2=8 m, and the width of the middle wing (inner bottom plate) is b_3=7.3 m. The thickness of the web and the upper and lower bottom plates are both 16 mm and the section height of the beam is $h = 3m$. The single-box, four-chamber, simply supported beam section has a span $L = 54m$, material of Q345E steel, elastic modulus $E = 2.06 \times 10^5 MPa$, and Poisson's ratio $\mu = 0.3$. Its cross-sectional dimensions are

shown in Figure 15. The flanges on the inner web of the beam act separately: concentrated load F=200 kN, uniform load q=50 kN/m, and beam section axial force N=500 kN. The area of the axial force is defined by the corresponding points A_1 and A_2 of the stiffener.
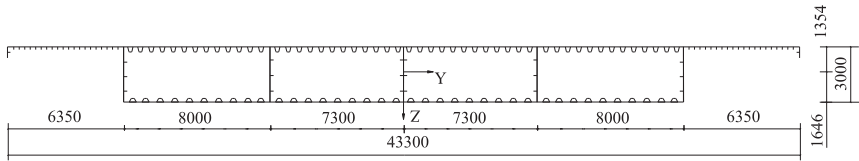
Figure 15: Single-box four-chamber steel box girder section (unit: mm)

The finite element model of the space plate and shell element was established under the above parameters. The box girder section stress under concentrated load "(a)" and uniform load "(b)" was calculated via the analogous rod method. The model is shown in Figure 16.
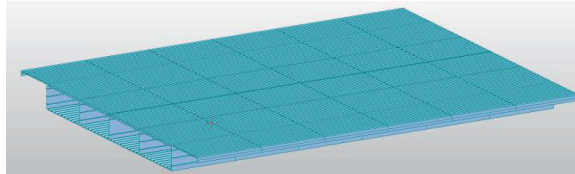
Figure 16: Steel box girder space plate element model

The stress comparison of the mid-span section is as follows.

Table 2: Cross-section stress in mid-span (unit: MPa)

Load type	(a) Uniform load			(b) Concentrated load		
Stiffener corresponding point	Theoretical solution	Data analysis	Errors	Theoretical solution	Data analysis	Errors
A1	1.01	1.13	11.8%	3.12	3.30	5.8%
A2	1.70	1.52	10.6%	3.53	3.39	3.9%
A3	0.50	0.57	14.0%	2.74	3.01	9.9%

As shown in Table 2, under the influence of loads (a) and (b), the theoretical analysis results are in close agreement with the finite element analysis results. It is feasible to use the analogous rod method to analyze the box girder section stress under compressive and bending loads.

7. Conclusion

The control section of the steel box girder of a self-anchored suspension bridge was analyzed in this study before versus after the system conversion in the construction stage. The longitudinal shear lag effect under different loads at the completion stage were analyzed as well. The cross-section stress of the girder under compressive and bending loads was deduced by the analogous rod method. The conclusions can be summarized as follows.

(1) During the construction stage, the bridge is transformed from a multi-span continuous system to a self-anchored suspension system. The shear lag coefficient of the main girder steel box girder changes significantly in the side cable anchorage area and the bridge tower before versus after the system conversion due to the different stress mechanisms of the two.

(2) In the bridge completion stage, under the action of uniformly distributed load, the shear lag coefficients at the side support, side cable anchorage area, and bridge tower position of the steel box girder change significantly. Under the action of concentrated load, positive and negative shear lag act in tandem on the anchorage area of the side cable at the support. Under an eccentric load, there are sudden changes in the shear lag coefficient at the support, the side cable anchorage area, and the junction of the positive and negative stress values. The shear lag coefficient in each span tends to be stable.

(3) A theoretical analysis of the shear lag effect on girder under compressive and bending loads was also carried out using the analogous rod method. It was assumed that the stiffening bar in the compression range bears axial force, the thin plate transmits shear force, and the vertical shear force acting on the section is borne by the web. The shear lag effect of the statically determinate structure was solved by deriving differential equations. The theoretical results and finite element analysis results are in agreement.

References

[1]   Z. Li, J. G. Nie, W. Y. Ji, "Positive and negative shear lag behaviors of composite twin-girder decks with varying cross-section," Science China Technological Sciences, vol. 60, no. 1, pp. 116-132, 2017.
[2]   S. J. Zhou, "Finite beam element considering shear-lag effect in box girder," Journal of Engineering Mechanics, vol. 136, no. 9, pp. 1115-1122, 2010.
[3]   Z. Li, R. K. L. Su, "Analytical solutions for composite beams with slip, shear-lag and time-dependent effects," Engineering Structures, vol. 152, pp. 559-578, 2017.
[4]   Q. Z. Luo, Y. M. Wu, Q. S. Li, "A finite segment model for shear lag analysis," Engineering Structures, vol. 26, no. 14, pp. 2113-2124, 2004.
[5]   S. T. Chang,, Q. Zhang, & S. Zhang, "Shear Lag Effect in Single Plane Cable-Stayed Bridge," Advances in Structural Engineering, vol. 1, no. 4, pp. 301-306, 1998.
[6]   G. Wu, X. Hong, "Theoretical and experimental study on shear lag effect of partially cable-stayed bridge," Journal of Zhejiang University Science A, vol. 6, pp. 875-877, 2005.
[7]   B. Atmaca, S. Ates, "Construction stage analysis of three-dimensional cable-stayed bridges," Steel and Composite Structures, vol. 12, no. 5, pp. 413-426, 2012.

[8]   S. W. Park, M. R. Jung, D. J. Min, M. Y. Kim, "Construction Stage Analysis of Cable-Stayed Bridges Using the Unstrained Element Length Method," Journal of The Korean Society of Civil Engineers, vol. 36, no. 6, pp. 991-998, 2016.

[9]   M. Gunaydin, S. Adanur, A. C. Altunisik, B. Sevim, E. Turker, "Determination of structural behavior of Bosporus suspension bridge considering construction stages and different soil conditions," Steel and Composite Structures, vol. 17, no. 4, pp. 405-429, 2014.

[10] B. S. Guo, W. He, Y. M. Yan. "Calculation of shear lag effect on thin-walled box girder by considering arrangement of stiffening rib," Journal of Xi'an University of Science and Technology, vol 32,no. 5, pp.617-620, 2012.

[11] Y. Zhao, B. Liu. "Test and analysis of shear lag for continuous steel bridge with large curvature." Journal of Xi'an University of Science and Technology," vol. 26, no. 3,pp.311-316, 2006.

[12] S. F. Zhu, Z. Y. Shu, C.J. Li. "Impact factor research on shear lag effect of PC composite box-girders with corrugated steel webs. Highway Engineering," vol. 39,no. 3, pp. 267-270, 2014.

[13] X. Wei, S. Y. Yang, "Research on the shear-lag effect in twin-cell PC box-girder with corrugated steel web," Journal of Railway Engineering Society, vol. 222, no. 3, pp. 29-33, 2017.

[14] Y. C. Zhou, X. W. Hao, Z. Q. Li, "Shear lag effect of non-uniform composite beam with corrugated steel web," Journal of Chang'an University(Nature Science Edition), vol.34, no. 3, pp. 62-68, 2014.

[15] C. Ma, S. Z. Liu, M. Y. Feng, "Variation method for shear lag effect of PC composite box girder with corrugated steel webs," Journal of Lanzhou Jiao-tong University, vol. 34,no. 11, pp. 22-32, 2018.

[16] Y. Chen, J. Dong, T. Xu, et al, "The shear-lag effect of composite box girder bridges with corrugated steel webs and trusses," Engineering Structures, vol. 181,pp. 617-628, 2019.

[17] J. B. Zou, R. D. Zhao, "Influence of support manners on shear lag effect of PC curved box girder with corrugated steel webs," Railway Engineering, vol. 58,no.8, pp. 7-9, 2018.

[18] Y. S. Ni, Y. Ma, D. Xu, et al, "Space mesh analysis method for shear lag effect of cable-stayed bridge with corrugated steel webs," Journal of Jilin University(Engineering and Technology Edition), vol. 47,no.5, pp. 1453-1464, 2017.

[19] J. Sa-nguanmanasak, T. Chakslmphob, E. Yamaguchi, "Stress concentration due to shear lag in continuous box girders," Engineering Structures, vol. 29 no.7, pp. 1414-1421, 2007.

[20] Q. G. Song, "Scordelis A C. Shear-lag analysis of T-, I-, and box beams," Journal of Structural Engineering, vol. 116, no. 5, pp. 1290-1305, 1990.

[21] S. I. Kundalwal, M. C. Ray, "Shear lag analysis of a novel short fuzzy fiber-reinforced composite," Acta Mechanica, vol. 225, no. 9, pp. 2621-2643, 2014.

[22] F. Gara, G. Ranzi, G. Leoni, "Short-and long-term analytical solutions for composite beams with partial interaction and shear-lag effects," International Journal of Steel Structures, vol. 10, no. 4, pp. 359-372, 2010.

[23] W. B. Zhou, L. Z. Jiang, Z. W. Yu, "Analysis of free vibration characteristic of steel-concrete composite box-girder considering shear lag and slip," vol. 20, no. 9, pp. 2570-2577, 2013.